Journal of Atmospheric Chemistry **41:** 281–296, 2002.

Fast-J2: Accurate Simulation of Stratospheric Photolysis in Global Chemical Models

HUISHENG BIAN and MICHAEL J. PRATHER
Earth System Science Department, University of California, Irvine, CA 92697-3100, U.S.A., e-mail: HBian@uci.edu and MPrather@uci.edu

(Received: 12 June 2001; in final form: 9 August 2001)

Abstract. Modeling photochemistry in the stratosphere requires solution of the equation of radiative transfer over an extreme range of wavelengths and atmospheric conditions, from transmission through the Schumann–Runge bands of O_2 in the mesosphere, to multiple scattering from tropospheric clouds and aerosols. The complexity and range of conditions makes photolysis calculations in 3-D chemical transport models computationally expensive. This study pesents a fast and accurate numerical method, Fast-J2, for calculating photolysis rates (J-values) and the deposition of solar flux in stratosphere. Fast-J2 develops an optimized, super-wide 11-bin quadrature for wavelengths from 177 to 291 nm that concatenates with the 7-bin quadrature (291–850 nm) already developed for the troposphere as Fast-J. Below 291 nm the effects of Rayleigh scattering are implemented as a pseudo-absorption, and above 291 nm the full multiple-scattering code of Fast-J is used. Fast-J2 calculates the mean ultraviolet-visible radiation field for these 18 wavelength bins throughout the stratosphere, and thus new species and new cross sections can be readily implemented. In comparison with a standard, high-resolution, multiple-scattering photolysis model, worst-case errors in Fast-J2 do not exceed 5% over a wide range of solar zenith angles, altitudes (0–60 km), latitudes, and seasons where the rates are important in photochemistry.

Key words: photolysis rates, stratospheric chemistry, chemical transport modeling.

1. Introduction

Throughout the stratosphere, chemistry is driven by solar radiation from the visible to the ultraviolet that photolyzes molecules. The intensity of this radiation and the resulting photolysis rates (J-values) vary greatly throughout the stratosphere, depending on wide-ranging atmospheric conditions such as overhead columns O_2 and O_3, solar zenith angle, pressure, temperature, stratospheric aerosols, and even tropospheric clouds and surface albedo. In 3-D chemistry-transport models (CTMs) therefore, the stratospheric J-values must be recalculated for every location at each time step, becoming an important part of the computational cost of stratospheric CTMs. The in-line calculation of photolysis rates has proven so expensive that most models have turned to lookup tables, off-line radiative transfer models, or other parametric fits for both tropospheric (e.g., Lefevre *et al.*, 1994; Berntsen and Isaksen, 1997; Roelofs *et al.*, 1997; Barth *et al.*, 2000) and stratospheric CTMs (e.g., Rasch *et al.*, 1995; Kaminski *et al.*, 1996; Zhao and Turco, 1997; Landgraf and

Crutzen, 1998; Bregman *et al.*, 2000; Kinnison *et al.*, 2001). This paper presents a new algorithm and program, Fast-J2, for fast and accurate calculation of photolysis rates throughout the stratosphere that can be readily used in-line with CTMs or general circulation models. It is an extension of the tropospheric Fast-J (Wild *et al.*, 2000), coupling the original scattering code at long wavelengths (291–850 nm) with an extinction code at short wavelengths (177–291 nm).

Fast-J2 uses a wide-band quadrature to integrate over the minimum possible number of wavelength bins and to perform scattering calculations only where needed. The quadrature is optimized to the wavelength structure of the absorbing species (O_2 and O_3) and does not depend on the wavelength structure of other photolyzed species. This new wide-band quadrature applies the principles of opacity distribution functions (ODF) – used for the Schumann–Runge (S–R) bands (Fang *et al.*, 1974) or the *k*-distribution method (Lacis and Oinas, 1991) – to the entire 177–291 nm interval, grouping disconnected wavelength intervals that have similar opacities. Cross section tables for current recommendations (DeMore *et al.*, 1997; Sander *et al.*, 2000) are supplied; however, new or updated photolysis rates can be readily calculated by suitably averaging high-resolution cross sections over Fast-J2's extended wavelength bins. The Fast-J2 program is shown to be accurate compared to the more detailed photolysis codes, and it reduces computation for the short wavelengths by more than a factor of ten.

Overall model structure is described in Section 2, including tests of the reference and standard UCI radiative transfer models. Methods of optimizing Fast-J2 within the prescribed error range of 5% are discussed in Section 3. Applicability and availability of the Fast-J2 code are summarized in Section 4.

2. Models of Stratospheric Photolysis

Our model for stratospheric and tropospheric photolysis covers the solar spectrum from 177 to 850 nm. Wavelengths less than 177 nm are attenuated above 60 km, and those >850 nm play no known role in photochemistry. Wavelengths greater than 291 nm reach into the troposphere where clouds, aerosols, surface albedo, and multiple scattering are important in determining the stratospheric photolytic radiation field; whereas the radiation field for those <291 nm depends predominantly on the overhead column of absorbers and scatterers.

The UCI reference model is developed with 10 cm^{-1} resolution, approximately 4500 wavelengths bin, from 177 to 850 nm, except in the Schumann–Runge (S–R) bands where O_2 cross section and solar flux are correlated with 0.5 cm^{-1} resolution (Minschwaner *et al.*, 1993). The solar spectrum at high resolution is taken from AFGL (Gail P. Anderson, private communication; Meier *et al.*, 1997) and the cross section for individual gases are based on the JPL-97/JPL-00 tabulated values (DeMore *et al.*, 1997; Sander *et al.*, 2000) interpolated to 10 cm^{-1} intervals with cubic splines. Where data are reported, cross sections are evaluated at different temperatures, and a linear interpolation between the observed range of temperatures is

used. For the reference model, the calculation of the atmospheric radiation field adopts a plane-parallel scattering atmosphere with a spherical ray-trace of the incoming solar beam and includes O_2 absorption, O_3 absorption, molecular Rayleigh scattering, a simple aerosol absorption and scattering. Scattering is included with a 6-stream Feautrier multiple-scattering calculation (Prather, 1974). The absorption cross sections for O_2 and O_3 depend on temperature and are evaluated locally using the temperature at each altitude level in the model. For practicality, these cross sections, including the S–R ODFs, are pre-evaluated at three temperatures (180, 260, and 300 K), and linear interpolation is used. For the other 53 photolyzed species, only two temperature vaules have been implemented here.

The UCI standard photolysis model is developed from the UCI reference model by averaging these 10 cm^{-1} solar fluxes and cross sections over larger wavelength bins. The S–R bands, from 177.49 to 202.5 nm, are treated individually from S–R(0,0) to S–R(14,0) with separate ODFs (Fang *et al.*, 1974; Minschwaner *et al.*, 1993). The S–R ODF intervals in the standard model are summarized in Table I. Photolysis of NO via the δ(0–0) band is located in S–R(5–0), and that via the δ(1–0) band is in S–R(9–0) and (10–0). The model calculates J(NO) using the S–R ODFs and partitioning the NO δ-band strengths among the appropriate S–R bands (e.g., Minschwaner and Siskind, 1993) with the effective mean cross section for each ODF interval given in Table I. The cross sections for gases other than O_2 and NO are averaged over these 15 S–R bands using the 10 cm^{-1} reference calculation to weight by solar flux and assuming that the species cross sections are not correlated with those of O_2. Including these 15 S–R bands, there are in total 77 wavelength bins of irregular width from 177.5 nm to 850 nm, see Table I. The choice of these 77 bins in the UCI standard model was made minimize the difference between J-values calculated with the standard model and those from the 10 cm^{-1} reference model: the two sets of J-values agree to within 1% over all altitudes (0–80 km) where they are photochemically important. This basic photolysis code has been described and applied to stratospheric examples (Prather and Remsberg, 1993; Avallone and Prather, 1997) and is closely related to several others that have been bested extensively against observed J-values and other models (e.g., Kelly *et al.*, 1995; Olson *et al.*, 1997; Gao *et al.*, 2001).

The Fast-J2 model is developed from the tropospheric Fast-J code (Wild *et al.*, 2000) plus this standard model to add the shorter wavelengths so that stratospheric J values can be computed. The short wavelength bin from the original Fast-J covered 289 to 298 nm. With the development of Fast-J2, this bin has been adjusted to 291–298 nm to provide the optimal interface with the stratospheric attenuation calculations. Fast-J2 uses the 8-stream, anisotropic multiple-scattering code from Fast-J for bins 12 through 18 (291–850 nm) and a simple exponential attenuation with optical depth for the short-wavelengths (bins 1–11, 177–291 nm).

Table I. UCI standard photolysis model

Bin no.	S–R band	Wavelength interval (nm)	Solar[a] flux (10^{11})	ODF intervals (fraction of solar flux) 1	2	3	4	5	6
1	(14,0)	177.49–178.30	1.021	0.0548	0.0550	0.1312	0.2819	0.2435	0.2336
2	(13,0)	178.30–179.26	1.443	0.0449	0.0634	0.1539	0.2485	0.2948	0.1945
3	(12,0)	179.26–180.38	1.624	0.0215	0.0537	0.0640	0.2584	0.3433	0.2591
4	(11,0)	180.38–181.65	2.130	0.0138	0.0262	0.0448	0.2361	0.3759	0.3032
5	(10,0)	181.65–183.08	2.998	0.0163	0.0340	0.1024	0.2037	0.3901	0.2535
6	(9,0)	183.08–184.65	2.927	0.0283	0.0649	0.0979		0.3058	0.2564
7	(8,0)	184.65–186.37	3.082	0.0424	0.0867	0.2068	0.3031	0.1845	0.1765
8	(7,0)	186.37–188.24	4.764	0.1008	0.1231	0.2430	0.3039	0.1390	0.0902
9	(6,0)	188.24–190.25	6.148	0.0680	0.1083	0.2504	0.3684	0.1569	0.0480
10	(5,0)	190.25–192.42	7.709	0.0511	0.1058	0.2874	0.2992	0.1641	0.0924
11	(4,0)	192.42–194.73	9.202	0.0662	0.1715	0.2809	0.1923	0.1407	0.1484
12	(3,0)	194.73–197.20	13.45	0.2762	0.2468	0.2104	0.1906	0.0760	
13	(2,0)	197.20–198.50	7.771	0.2570	0.2498	0.1980	0.1976	0.0976	
14	(1,0)	198.50–200.00	9.632	0.5138	0.2429	0.1415	0.1018		
15	(0,0)	200.00–202.50	19.31	0.6147	0.3386	0.0467			

Bin	S–R	X[NO] $*$ (10^{-18}) 1	2	3	4	5	6
5	(10,0)	17.8	15.1	16.7	10.9	7.85	2.97
6	(9,0)	0.0	0.0	0.0	0.0	2.40	6.37
10	(5,0)	0.0	1.86	3.66	3.84	2.80	4.62

Bin	Interval (nm)	Bin	Interval (nm)	Bin	Interval (nm)
16	202.5–204.0	38	289.0–291.0	60	315.7–317.2
17	204.0–206.5	39	291.0–293.0	61	317.2–318.7
18	206.5–209.5	40	293.0–295.0	62	318.7–320.3
19	209.5–212.5	41	295.0–296.8	63	320.3–322.5
20	212.5–215.5	42	296.8–298.3	64	322.5–327.0
21	215.5–218.5	43	298.3–299.6	65	327.0–335.0
22	218.5–221.5	44	299.6–300.5	66	335.0–345.0
23	221.5–225.0	45	300.5–301.5	67	345.0–355.0
24	225.0–229.0	46	301.5–302.5	68	355.0–365.0
25	229.0–233.0	47	302.5–303.5	69	365.0–375.0
26	233.0–237.5	48	303.5–304.5	70	375.0–390.1
27	237.5–242.5	49	304.5–305.5	71	390.1–412.5
28	242.5–248.0	50	305.5–306.5	72	412.5–437.6
29	248.0–254.0	51	306.5–307.5	73	437.6–485.1
30	254.0–260.0	52	307.5–308.5	74	485.1–560.1
31	260.0–265.5	53	308.5–309.5	75	560.1–635.1
32	265.5–270.5	54	309.5–310.5	76	635.1–760.2
33	270.5–275.5	55	310.5–311.5	77	760.2–850.0
34	275.5–280.0	56	311.5–312.5		
35	280.0–283.5	57	312.5–313.5		
36	283.5–286.5	58	313.5–314.5		
37	286.5–289.0	59	314.5–315.7		

Solar flux in each S–R band (bins 1–15) is given in units 10^{11} photons cm^{-2} s^{-1} per interval. The Opacity Distribution Function intervals (ranging from 3 to 6 per band) are sorted in order of increasing O_2 cross-section and give the fraction of the solar flux in each interval (sums to 1.0000 for each S–R band).

The underlined intervals for each S–R band contribute to photolysis below 60 km altitude and are included in the Fast-J2 super-ODFs (see Table II). The NO cross-sections (X[NO]) are given in units 10^{-18} cm^2 as the average over each ODF interval in the S–R bands (10,0), (9,0), and (5,0) with the underline notation as above. Bins 16–77 comprise the rest of the wavelengths used to calculate J-values.

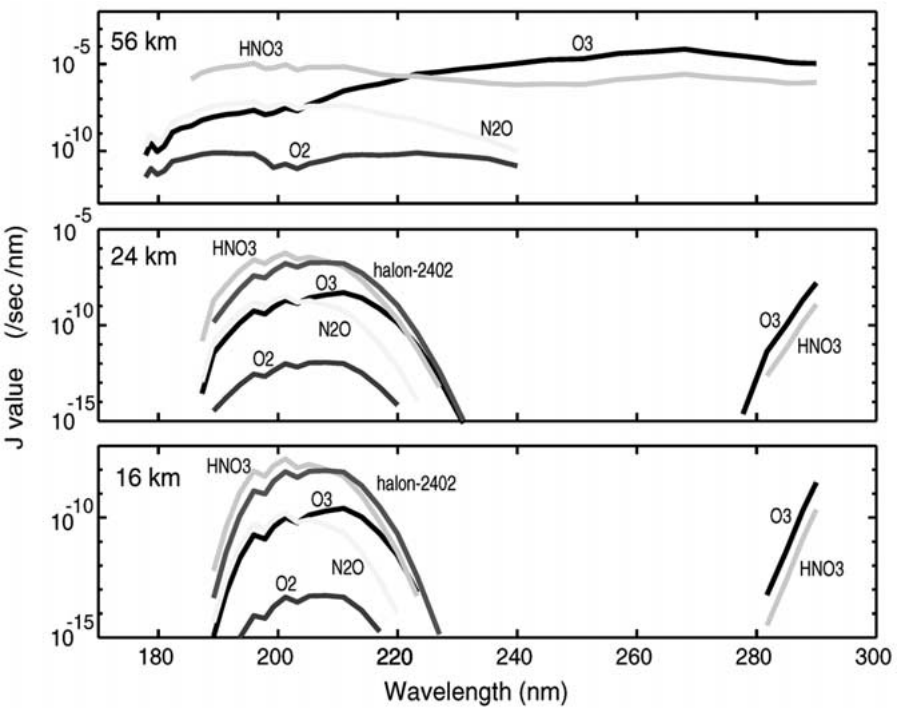

Figure 1. J-values (nm^{-1} sec^{-1}) for O_2, O_3, N_2O, halon-2402 ($C_2F_4Br_2$), and HNO_3, calculated as a function of wavelength over the region 177 to 291 nm for three different altitudes (56 km, 24 km, and 16 km). Calculations use overhead sun (SZA = 0°) with U.S. Standard Atmosphere.

3. Optimizing the Computation of Stratospheric Photolysis Rates

The variation of sunlight in the 177–291 nm region throughout the stratosphere involves rapid attenuation in the S–R bands at short wavelengths and in the ozone Hartley bands around 250 nm. Thus the wavelengths important for photolysis in the stratosphere shift from a broad contribution across 180–290 nm at 56 km altitude (Figure 1, top panel) to two window regions, 200–220 nm and 270–290 nm, in the lower stratosphere (lower panels, 24 km and 16 km). This pattern directs the approach in optimizing the wavelength quadrature as described below.

3.1. RAYLEIGH SCATTERING AS ABSORPTION

The ratio of total scattered flux to direct solar flux calculated by the standard UCI model using 6-stream Rayleigh-phase scattering compres well with observations data (Herman and Mentall, 1982; Minschwaner *et al.*, 1995a) and other model simulations (Kylling *et al.*, 1993; Minschwaner *et al.*, 1995b) as summarized in Figure 2. The standard model simulation uses only molecular scattering and matches the measurement very well in the wavelength range 200–320 nm. For

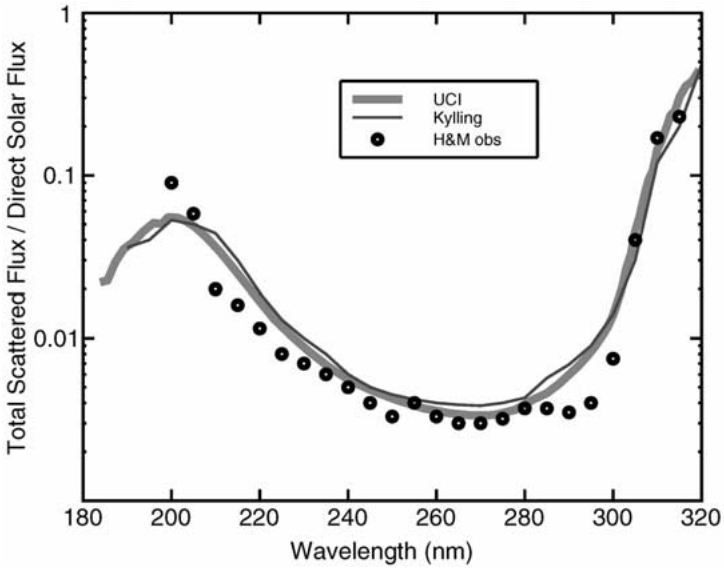

Figure 2. The ratio of total scattered flux to direct solar flux as a function of wavelength given by models and observation at 40 km and solar zenith angle of 41° from observations (points, Herman and Mentall, 1992), from the standard UCI model (thick line), and from Kylling *et al.* (1993).

wavelength less than 210 nm, our modeled ratio is clearly less than that of the Hermann and Mentall (1982) observations but is consistent with the more recent analysis of Minschwaner *et al.* (1995a). Therefore, the standard model has a good ability to simulate the atmospheric radiation field over this wavelength region, and we derive the Fast-J2 code from it.

Molecular Rayleigh scattering adds to the attenua tion of sunlight but does not absorb photons. Nevertheless, the scattering of 177–291 nm light upwards, or into more horizontal paths, leads to its absorption at higher altitudes and reduces the number of photons at lower altitudes. Thus, the effect of Rayleigh scattering is to reduce J-values in the lower stratosphere, while increasing them only slightly in the upper stratosphere. The relative importance of scattering with wavelength and with altitude is shown for the standard UCI model in Figure 3. Combining Figures 3 and 1, one can see that accurate treatment of Rayleigh scattering is essential in calculating photolysis rates at 24 km altitude and below.

An alternative to the full multiple-scattering calculation of the standard model would be to include Rayleigh-scattering effects somehow in a simple exponential attenuation model that depends only on the solar path (i.e., overhead optical depth divided by cosine of the solar zenith angle in a plane-parallel atmosphere). Thus, we define a pseudo-Rayleigh absorption cross section (% of the scattering cross section) that accounts for the loss of photolysis radiation in the lower stratosphere from Rayleigh scattering. Examples of the errors when Rayleigh scattering is ig-

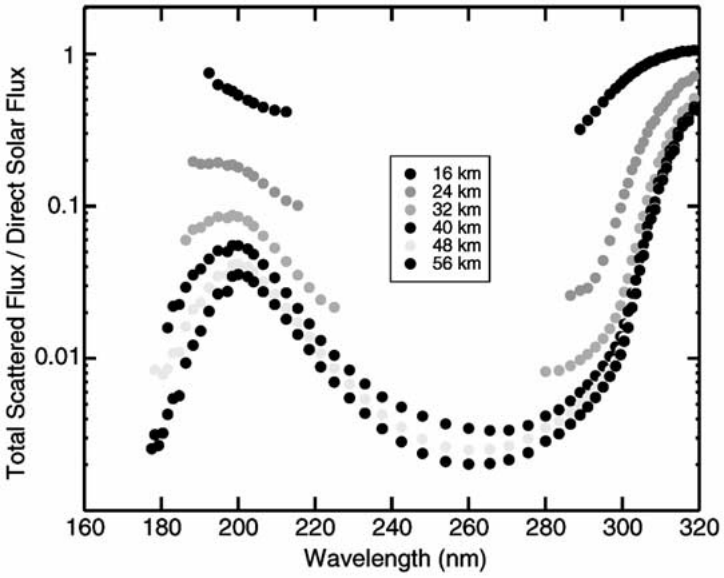

Figure 3. The ratio of total scattered flux to direct solar flux as a function of wavelength at different altitudes as calculated in the standard UCI model (clear sky, albedo = 0.3, SZA = 0°).

nored or treated as partial absorption are given in Figure 4 for J(N_2O). When scattering is ignored (green line), the J-value is about 3% too small in the upper stratosphere, but rapidly becomes too large below 30 km, with errors >10% below 24 km. When the pseudo-Rayleigh absorption cross section is taken as 100% (i.e., all absorption, blue line), the error in the upper stratosphere is still the same since there is no back-scattered radiation, but the error growth is opposite in the lower stratosphere and J-values rapidly become too small below 24 km. An optimal fit is found for a pseudo-Rayleigh absorption equal to 57% of the scattering cross section (red line), and the error in J(N_2O) remains almost constant at –3% for all altitudes down to 20 km. Similar results are obtained for a range of species, atmospheres, and solar zenith angles. Thus, within the adopted precision criteria of 5%, the effects of molecular scattering may be effectively treated as simple molecular absorption with a cross section 57% that of scattering.

3.2. GROUPING THE WAVELENGTH BINS

The standard UCI model has 38 bins from 177 nm to 291 nm that include separately the 15 individual S–R bands (14,0) through (0,0), and each bin has a relatively high wavelength resolution ranging from about 1 to 5 nm per bin (see Table I). This resolution was chosen to integrate accurately the product of solar flux and species' cross sections as compared to a reference case with resolution of about 0.05 nm (10 cm^{-1}). With Fast-J2, we adopt the 7 super-wide bins already developed for

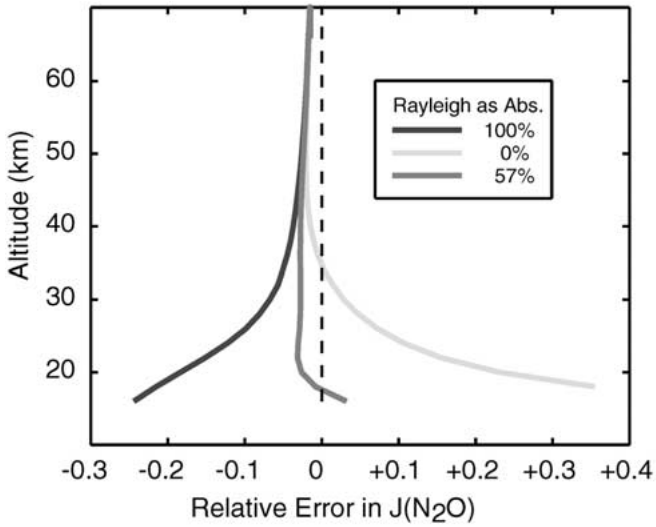

Figure 4. The relative error in $J(N_2O)$ (%) as a function of altitude calculated with Fast-J2 for different methods of treating Rayleigh scattering: Ignoring Rayleigh scattering (0%), including it as absorption (100%), and including a fraction (57%) as absorption. Errors are relative to standard UCI model and use a USAF reference atmosphere (5° N, October, SZA = 0°).

Fast-J to integrate over the standard model's 39 bins for 291–850 nm and search for a minimal set of super-wide bins to integrate accurately over the 177–291 nm region.

While the width of the standard bins can be further enlarged and still meet the 5% precision requirement for J-values, it became clear that substantial reductions could only be achieved if the wavelength regions were re-ordered over the whole wavelength region so as to group regions of similar absorption and hence attenuation (e.g., Fang *et al.*, 1974; Lacis and Oinas, 1991). Thus, the 15 S–R individual bands and their ODFs from the standard model are re-sorted according to O_2 cross section, and most are placed in the new super-wide bins numbered 1 to 5 in order of decreasing O_2 cross section (see Table II). The fraction of the solar flux in the specified S–R band given in Table II refers to the S–R wavelength ranges and solar fluxes listed in Table I. The window region of S–R(5,0), comprising about 16% of the solar flux, falls into super-bin number 8 along with the 212–215 nm continuum region, and the 202–206 nm continuum falls into super-bin 5 with the low-number S–R bands. Not all wavelength regions of the high-number S-R bands. Not all wavelength regions of the high-number S–R bands are represented here since wavelengths with very large O_2 cross sections do not contribute to photolysis below 60 km altitude. For example, only 24% of S–R(14,0) and 91% of S–R(5,0) are included in Fast-J2. These ODF intervals from the standard model that are included in Fast-J2 are designated by underlines in Table I. The NO δ-bands are now distributed across super-bins 1, 2, 3, and 8 (see Table III) with bin 8 including

Table II. Wavelength regions grouped into Fast-J2's 18 bins

Bin 01	S–R(14,0)	24.1%	S–R(13,0)	51.1%	S–R(12,0)	39.8%
	S–R(11,0)	32.1%	S–R(10,0)	20.4%	S–R(9,0)	55.3%
	S–R(8,0)	48.8%	S–R(7,0)	30.4%	S–R(6,0)	15.7%
	S–R(5,0)	16.4%	S–R(4,0)	14.8%	S–R(3,0)	7.6%
Bin 02	S–R(10,0)	15.3%	S–R(9,0)	19.1%	S–R(8,0)	33.6%
	S–R(7,0)	24.3%	S–R(6,0)	36.8%	S–R(5,0)	29.9%
	S–R(4,0)	33.3%	S–R(3,0)	19.1%	S–R(2,0)	9.8%
Bin 03	S–R(7,0)	22.4%	S–R(6,0)	42.7%	S–R(5,0)	28.7%
	S–R(4,0)	28.1%	S–R(3,0)	21.0%	S–R(2,0)	19.8%
	S–R(1,0)	10.2%	S–R(0,0)	4.7%		
Bin 04	S–R(4,0)	23.8%	S–R(3,0)	24.7%	S–R(2,0)	44.8%
	S–R(1,0)	14.2%				
Bin 05	S–R(3,0)	27.6%	S–R(2,0)	25.7%	S–R(1,0)	75.7%
	S–R(0,0)	95.3%	202.5–206.5 nm			
Bin 06	206.5–209.5 nm					
Bin 07	209.5–212.5 nm					
Bin 08	S–R(5,0)	15.7%	212.5–215.5 nm			
Bin 09	233.0–275.5 nm					
Bin 10	221.5–233.0 nm		275.5–286.5 nm			
Bin 11	215.5–221.5 nm		286.5–291.0 nm			
Bin 12 [a]	291.0–298.3 nm					
Bin 13 [a]	298.3–307.5 nm					
Bin 14 [a]	307.5–312.5 nm					
Bin 15 [a]	312.5–320.3 nm					
Bin 16 [a]	320.3–345.0 nm					
Bin 17 [a]	345.0–412.5 nm					
Bin 18 [a]	412.5–850.0 nm					

[a] The 7 original Fast-J bins, shifted to start at 291 nm.

the δ(0–0) lines in the second ODF interval of the S–R(5,0) and the contributions from the highest ODF intervals dropped as shown in Table I.

Where the O_3 cross section changes slowly near its maximum ($\sim$255 nm), a super-bin 9 (233–275 nm) can be defined with little loss of precision. An obvious re-grouping is the wavelength regions with similar O_3 cross sections on either side of this maximum, and this is done for the super-bins 10 and 11.

Table II summarizes the re-grouping of the S–R bands and the continuum regions longward of 202.5 nm. Table III gives the solar fluxes, absorption cross sections for O_2 and O_3 at 3 temperatures, plus some sample cross sections for other species' J-values using the 18 super-wide bins of Fast-J2. Since Fast-J2 calculates the mean photolytic intensity in each super-bin, the mean cross sections for other species are thus calculated as the flux-weighted average over all wavelength regions in each super-bin as defined in Table II. Cross sections in the S–R bands are first averaged over the wavelength range of each band given in Table I and then included in the super-bin with a weighting equal to the specified percentage of the S–R band (Table II) times the flux in that band (Table I). Cross sections in the continuum regin ($>$202 nm) are included in the super-bin with a weighting equal to the solar flux.

3.3. ERRORS IN FAST-J2

The errors induced by the approximation in Fast-J2 remain within the 5% design criterion. For example, the treatment of Rayleigh scattering as partial absorption is a small error (Figure 4). The re-ordering of the S–R bands does not induce significant error in the calculation of J(NO) as shown in Figure 5: the key regions for NO photolysis are above 30 km altitude, and the Fast-J2 errors are $<$5% for 30–60 km. (Note that these examples and the current formulation of the UCI standard model and Fast-J2 do not include the self-absorption by thermospheric NO.) The relative errors in J(CF_2Cl_2) are shown in Figure 6: the mean bias of –3% is from the approximation for Rayleigh scattering and remaining errors vary $\pm$3% about this. The errors exceed 5% only for very large air masses (e.g., 35 km with SZA = 80°) when the J-values are not usually important in terms of global stratospheric chemistry.

One concern about combining different wavelength regions applies to bins 10 and 11 that mix regions of similar O_3 cross sections but very different O_2 cross sections. If the variations in O_2 opacity were large and uncorrelated with that of O_3 then this approach would not work since different wavelengths within the bin would attenuate sunlight differently. Figure 7 shows the optical depths in O_2 and O_3 for the split bins 10 and 11 for a range of altitudes and solar zenith angles along with the Herzberg continuum bin 7 for comparison. In all these cases the O_3 optical depth dominates that of O_2, especially for bins 10 and 11, and the points fall along a line. Thus, this part of the Fast-J2 methodology should remain accurate in a typical stratoshere.

Table III. Solar fluxes (photons cm^{-2} s^{-1} bin^{-1}) and sample cross sections (cm^2) for Fast-J2's super-wide bins

Bin	Solar	O_2 cross section			O_3 cross section		
#	flux	180 K	260 K	300 K	180 K	260 K	300 K
1	1.211e+12	1.728e–21	2.268e–21	2.754e–21	5.862e–19	5.928e–19	5.895e–19
2	1.417e+12	1.990e–22	3.059e–22	4.239e–22	4.685e–19	4.772e–19	4.712e–19
3	1.474e+12	3.006e–23	4.913e–23	7.402e–23	4.130e–19	4.223e–19	4.150e–19
4	8.409e+11	9.843e–24	1.409e–23	2.102e–23	3.546e–19	3.648e–19	3.555e–19
5	7.218e+12	7.305e–24	7.688e–24	8.352e–24	3.228e–19	3.330e–19	3.301e–19
6	4.394e+12	6.835e–24	6.835e–24	6.835e–24	4.555e–19	4.610e–19	4.688e–19
7	8.905e+12	6.243e–24	6.243e–24	6.243e–24	6.287e–19	6.325e–19	6.372e–19
8	1.0930+13	5.789e–24	5.875e–24	5.974e–24	9.129e–19	8.753e–19	8.997e–19
9	6.1060+14	8.623e–26	8.623e–26	8.623e–26	8.866e–18	8.877e–18	8.882e–18
10	4.102e+14	4.745e–25	4.745e–25	4.745e–25	3.463e–18	3.563e–18	3.596e–18
11	3.090e+14	3.996e–25	3.996e–25	3.996e–25	1.494e–18	1.553e–18	1.596e–18
12	5.751e+14				7.480e–19	7.931e–19	8.305e–19
13	7.332e+14				2.365e–19	2.571e–19	2.777e–19
14	5.022e+14				8.722e–20	9.673e–20	1.075e–19
15	8.709e+14				3.694e–20	4.141e–20	4.725e–20
16	3.786e+15				4.295e–21	5.457e–21	6.782e–21
17	1.544e+16				1.804e–23	2.775e–23	4.824e–23
18	2.110e+17				1.630e–21	1.630e–21	1.630e–21

	Rayleigh	NO	HNO_3		Halons		
	scattering		200 K	300 K	CF_2ClBr	CF_3Br	$C_2F_4Br_2$
1	5.083e–25	1.021e–18	8.061e–18	8.174e–18	2.395e–19	2.971e–20	4.353e–19
2	4.468e–25	1.158e–18	1.088e–17	1.118e–17	5.088e–19	6.206e–20	8.892e–19
3	4.184e–25	5.498e–19	1.033e–17	1.082e–17	6.813e–19	7.949e–20	1.080e–18
4	3.904e–25		8.225e–18	9.106e–18	8.515e–19	9.572e–20	1.216e–18
5	3.355e–25		3.788e–18	4.473e–18	1.149e–18	1.169e–19	1.212e–18
6	2.929e–25		1.301e–18	1.565e–18	1.202e–18	1.231e–19	1.114e–18
7	2.736e–25		6.914e–19	8.458e–19	1.142e–18	1.166e–19	1.026e–18
8	2.580e–25	1.390e–20	4.946e–19	5.796e–19	1.046e–18	1.057e–19	9.191e–19
9	1.050e–25		1.631e–20	1.877e–20	3.790e–20	1.415e–21	2.556e–20
10	9.375e–26		1.743e–20	2.100e–20	8.360e–20	6.801e–21	6.912e–20
11	8.043e–26		1.802e–20	2.241e–20	7.307e–20	7.078e–21	6.250e–20
12	6.124e–26		3.371e–21	4.354e–21			
13	5.422e–26		1.377e–21	1.923e–21			
14	4.921e–26		5.451e–22	8.314e–22			
15	4.515e–26		2.102e–22	3.589e–22			
16	3.645e–26		2.154e–23	4.764e–23			
17	2.082e–26		8.105e–26	2.499e–25			
18	3.853e–27						

	N_2O		$CFCl_3$		CF_2Cl_2	
	200 K	300 K	200 K	295 K	210 K	295 K
1	1.064e–19	1.211e–19	2.123e–18	2.169e–18	9.598e–19	1.005e–18
2	8.304e–20	9.844e–20	1.526e–18	1.607e–18	4.975e–19	5.695e–19
3	6.784e–20	8.267e–20	1.222e–18	1.314e–18	3.151e–19	3.889e–19
4	5.019e–20	6.426e–20	8.888e–19	9.907e–19	1.462e–19	2.095e–19
5	2.100e–20	3.031e–20	4.293e–19	5.055e–19	3.664e–20	6.214e–20
6	6.196e–21	1.110e–20	1.688e–19	2.125e–19	6.384e–21	1.416e–20
7	3.137e–21	6.355e–21	1.004e–19	1.301e–19	2.484e–21	6.114e–21
8	2.400e–21	4.533e–21	7.257e–20	9.250e–20	5.462e–21	8.329e–21
9	3.114e–25	1.418e–24	5.665e–23	9.613e–23	1.368e–25	7.614e–25
10	9.720e–24	3.765e–23	7.925e–22	1.185e–21	7.347e–24	2.823e–23
11	4.035e–23	1.148e–22	2.019e–21	2.811e–21	2.750e–23	8.654e–23

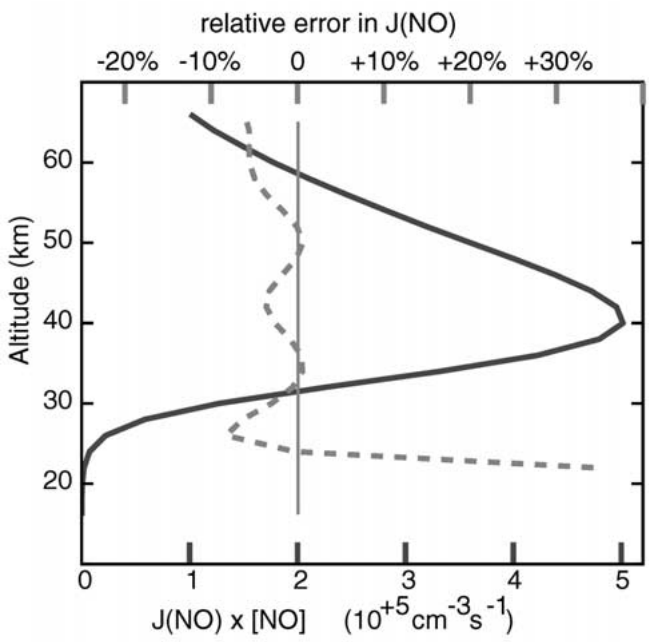

Figure 5. The relative error in 24-hour average J(NO) (%, top axis, red dashed line) as a function of altitude calculated with Fast-J2 (compared with UCI standard model, see Figure 4). Also shown is a sample calculation of the 24-hour average calculation of the NO photolysis rate (10^5 cm^{-3} s^{-1}) to show altitude region of photochemical importance for this J-value.

4. Summary and Caveats

Our fast stratospheric photolysis model, Fast-J2, uses 11 super-wide, opacity-sorted bins to describe the mean radiation field in the wavelength range 177 to 291 nm. It accounts for Rayleigh scattering with pseudo-absorption that is accurate to a few percent. For wavelengths greater than 291 nm, it uses the tropospehric Fast-J code (Wild *et al.*, 2000). Compared with the standard model from which it was derived, Fast-J2 is accurate to 5% over a wide range of altitudes, solar zenith angles, latitudes and seasons where the photolysis rates are important to stratospheric chemistry. Because of the treatment of Rayleigh scattering, these errors tend to be systematic and negative, e.g., Fast-J2 is typically 3% lower than the reference model for source gases like N_2O. Although one could offset the J-values to account for this, no attempt is made here to correct this type of error. Compared with the standard UCI model, Fast-J2 computes photolysis rates more than ten times faster.

The results here could be easily applied to other photochemical models. The choice of wavelength intervals is robust and would only need to be re-evaluated if there were a substantial change in the O_2 or O_3 cross sections. Adding or revising J-values for other species is trivial: one needs only to calculate the mean cross sectiosn for the Fast-J2 super-bins as the solar-flux-weighted averages over the

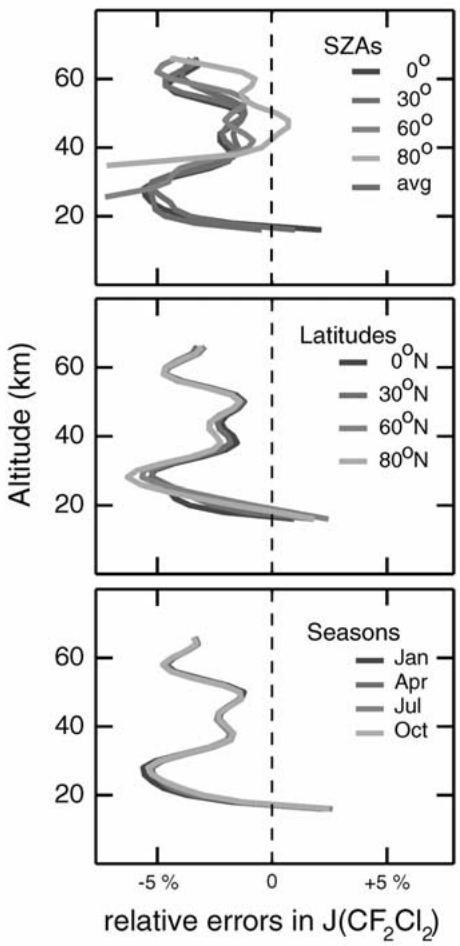

Figure 6. The relative error in $J(CF_2Cl_2)$ (%) as a function of altitude calculated with Fast-J2 (compared with UCI standard model). Results are shown for (a) a range of solar zenith angles (SZA) and their 24-hour average with the U.S. Standard Atmosphere, (b) a range of latitudes in April (USAF reference atmospheres) with overhead sun, and (c) a range of seasons at 30° N with overhead sun. The latter two cases show only the sensitivity to changes in the background atmosphere.

wavelength ranges for each super-bin given in Table II, treating the S–R band fractions as a wavelength range per previous discussion.

Fast-J2 is not designed for conditions with very large aerosol loading in the stratosphere, e.g., the first months of the Pinatubo cloud. In such circumstances, the code would have to be adjusted to calculate the 11 short-wavelength bins with full multiple scattering as in the Fast-J code. Also, the wavelength optimization has been designed for conditions of typical high-sun, active photochemistry; and hence caution and further tests would be needed before Fast-J2 is applied to studies of the winter polar stratosphere with twilight photochemistry.

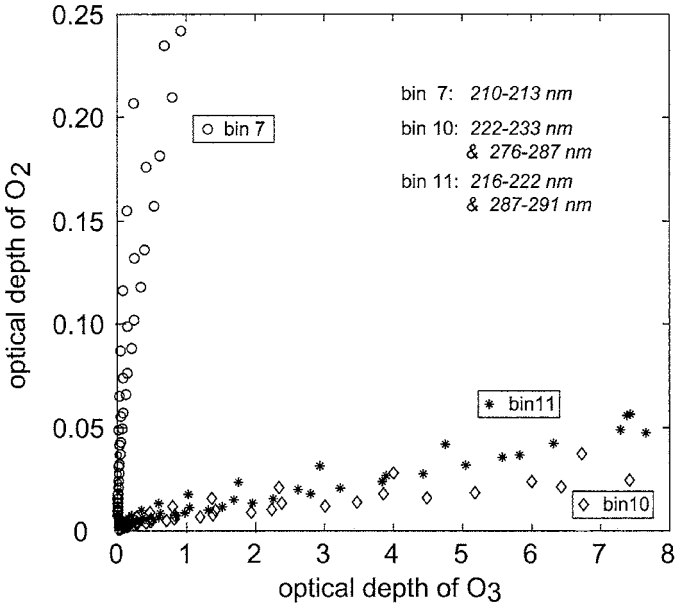

Figure 7. Slant-column optical depths in O_2 and O_3 to the sun, sampled from the different stratospheric altitudes (16–80 km) and different SZA 0°–80° for a January tropical atmosphere. Results are shown for the three super-wide bins of Fast-J2 (nos. 7, 10, and 11) that include both O_2 and O_3 absorption. The tight correlation for each bin demonstrates that the relative amounts of attenuation by these two absorbers remains nearly constant over a wide range of conditions.

The Fast-J2 code is available from the authors of this paper or the Fast-J paper, check the UCI Earth System Science Department web site for details (http://ess.uci.edu/~prather).

Acknowledgements

The authors wish to acknowledge the assistance of Xin Zhu and Oliver Wild in the development of Fast-J2 and the two anonymous reviewers whose comments improved the manuscript. This work was supported in part by the NASA Atmospheric Chemistry Modeling and Analysis Program and the NSF Atmospheric Chemistry Program.

References

Avalonne, L. M. and Prather, M. J., 1997: Tracer-tracer correlations: Three-dimensional model simulations and comparisons to observations, *J. Geophys. Res.* **102**, 19233–19246.

Barth, M. C., Rasch, P. J., Kiehl, J. T., Benkovitz, C. M., and Schwartz, S. E.: 2000, Sulfur chemistry in the NCAR CCM: Description, evaluation, features, and sensitivity to aqueous chemistry, *J. Geophys. Res.* **105**, 1387–1415.

Berntsen, T. K. and Isaksen, I. S. A., 1997: A global three-dimensional chemical transport model for the troposphere 1, model description and CO and ozone results, *J. Geophys. Res.* **102**, 21239–21280.

Bregman, A., Lelieveld, J., van den Broek, M. M. P., Siegmund, P. C., Fischer, H., and Bujok, O., 2000: N_2O and O_3 relationship in the lowermost stratosphere: a diagnostic for mixing processes as represented by a three-dimensional chemistry-transport model, *J. Geophys. Res.* **105**, 17279–17290.

DeMore, W. B., Sander, S. P., Goldan, D. M., Hampson, R. F., Kurylo, M. J., Howard, C. J., Ravishankara, A. R., Kolb, C. E., and Molina, M. J., 1997: Chemical kinetics and photochemical data for use in stratospheric modeling, evaluation no. 12, JPL Publication 97-4, Jet Propulsion Laboratory, California Institute of Technology, Pasadena.

Fang, T. M., Wofsy, S. C., and Dalgarno, A., 1974: Opacity distribution functions and absorption in Schumann–Runge bands of molecular-oxygen, *Planet. Spa. Sci.* **22**, 413–425.

Gao, R. S. et al., 2001: J(NO_2) at high solar zenith angles in the lower stratosphere, *Geophys. Res. Lett.* **28**, 2405–2408.

Herman, J. R. and Mentall, J. E., 1982: The direct and scattered solar flux within the stratosphere, *J. Geophys. Res.* **87**, 1319–1330.

Kaminski, J. W., McConnell, J. C., and Boville, B. A., 1996: A three-dimensional chemical transport model of the stratosphere: Midlatitude results, *J. Geophys. Res.* **101**, 28731–28751.

Kelley, P., Dickerson, R. R., Luke, W. T., and Kok, G. L., 1995: Rate of NO_2 photolysis from the surface to 7.6-km altitude in clear-sky and clouds, *Geophys. Res. Lett.* **22**, 2621–2624.

Kinnison, D. E. et al., 2001: The global modeling initiative assessment model: Application to high-speed civil transport perturbation, *J. Geophys. Res.* **106**, 1693–1712.

Kylling, A., Stamnes, K., Meier, R. R., and Anderson, D. E., 1993: The 200-nm to 300-nm radiation-field in the stratosphere – comparison of models with observation, *J. Geophys. Res.* **98**, 2741–2745.

Lacis, A. A. and Oinas, V., 1991: A description of the correlated kappa-distribution method for modeling nongray gaseous absorption, thermal emission, and multiple-scattering in vertically inhomogeneous atmospheres, *J. Geophys. Res.* **96**, 9027–9063.

Landgraf, J. and Crutzen, P. J., 1998: An efficient method for online calculations of photolysis and heating rates, *J. Atmos. Sci.* **55**, 863–878.

Lefevre, F., Brasseur, G. P., Folkins, I., Smith, A. K., and Simon, P., 1994: Chemistry of the 1991–1992 stratospheric winter – 3-dimensional model simulations, *J. Geophys. Res.* **99**, 8183–8195.

Meier, R. R., Anderson, G. P., Cantrell, C. A., Hall, L. A., Lean, J., Minschwaner, K., Shetter, R. E., Shettle, E. P., and Stamnes, K., 1997: Actinic radiation in the terrestrial atmosphere, *J. Atmos. Solar-Terr. Phys.* **59**, 2111–2157.

Minschwaner, K. and Siskind, D. E., 1993: A new calculation of nitric-oxide photolysis in the stratosphere, mesosphere, and lower thermosphere, *J. Geophys. Res.* **98**, 20401–20412.

Minschwaner, K., Salawitch, R. J., and McElroy, M. B., 1993: Absorption of solar-radiation by O_2-implications for O_3 and lifetimes of N_2O, $CFCl_3$, and CF_2Cl_2, *J. Geophys. Res.* **98**, 10543–10561.

Minschwaner, K., Thomas, R. J., and Rusch, D. W., 1995a: Scattered ultraviolet radiation in the upper stratosphere, 1, Observations, *J. Geophys. Res.* **100**, 11157–11164.

Minschwaner, K., Anderson, G. P., Hall, L. A., Chetwynd, J. H., Thomas, R. J., Rusch, D. W., Berk, A., and Conant, J. A., 1995b: Scattered ultraviolet-radiation in the upper-stratosphere, 2, models and measurements, *J. Geophys. Res.* **100**, 11165–11171.

Olson, J. *et al.*, 1997: Results from the IPCC photochemical model intercomparison (PhotoComp), *J. Geophys. Res.* **102**, 5979–5991.

Prather, M. J., 1974: Solution of the inhomogeneous Rayleigh scattering atmosphere, *Astrophys. J.* **192**, 787–792.

Prather, M. J. and Remsberg, E. E. (eds), 1993: Chapter 4. GISS Photochemical Model, in *Report of the 1992 Stratospheric Models and Measurements Workshop*, Satellite Beach, FL, February 1992, NASA Ref. Publ., pp. 76–85.

Rasch, P. J., Boville, B. A., and Brasseur, G. P., 1995: A 3-dimensional general-circulation model with coupled chemistry for the middle atmosphere, *J. Geophys. Res.* **100**, 9041–9071.

Roelofs, G. J., Lelieveld, J., and Vandorland, R., 1997: A three-dimensional chemistry general circulation model simulation of anthropogenically derived ozone in the troposphere and its radiative climate forcing, *J. Geophys. Res.* **102**, 23389–23401.

Sander, S. P., Friedl, R. R., DeMore, W. B., Ravishankara, A. R., Golden, D. M., Kolb, C. E., Kurylo, M. J., Hampson, R. F., Huie, R. E., Molina, M. J., and Moortgat, G. K., 2000: Chemical kinetics and photochemical data for use in stratospheric modeling, supplement to evaluation no. 12 – Update of key reactions and evaluation no. 13, JPL Publication 00-3, Jet Propulsion Laboratory, California Institute of Technology, Pasadena.

Wild, O., Zhu, X., and Prather, M. J., 2000: Fast-J: Accurate simulation of in- and below-cloud photolysis in tropospheric chemical models, *J. Atmos. Chem.* **37**, 245–282.

Zhao, X. P. and Turco, R. P., 1997: Photodissociation parameterization for stratospheric photochemical modeling, *J. Geophys. Res.* **102**, 9447–9459.